Support Information for:

The difunctional applications of modified $Sr_2YbF_7:Tm^{3+}$ upconversion nanocrystals

Li-Jun Xiang, Hui-Hui Zhang, Hong Li, Lin Kong, Hong-Ping Zhou, Jie-Ying Wu, Yu-Peng Tian, Jie Zhang and Yi-Fu Mao

Content

S1 Experimental

S1.1 Materials

$SrCl_2$ (99.99%) and $Ln(NO_3)_3·6H_2O$ (Ln = Yb, Tm) were purchased from Sigma-Aldrich. Poly (ethylene glycol) methyl ether (PEG, average molecular = 6000) was purchased from Sinopharm Chemical Reagent Co., China. Other chemicals are of analytical grade and used as received without further purification.

S1.2 Synthesis of $(1-x)SrF_2•xYbF_3$ NCs

The NCs were prepared with oleic acid as capping ligand through a simple solvothermal method. In detail, 10.5 mmol NaOH, 10 mL alcohol and 20 mL oleic acid were firstly added into a beaker in turn under vigorous agitation to form transparent homogeneous solution. Then, (1-*x*) mmol $SrCl_2$ (1 M) and *x* mmol $Yb(NO_3)_3$ (1 M) aqueous solution were introduced into the former solution. At last, 4 mmol NH_4F (1 M) deionized water solution was added, and the mixture was vigorously stirred for 30 min. The mixture was transferred into a 50 mL stainless teflon-lined autoclave, and heated at 200 ^oC for 24 h. Then, cooled down to room temperature. The products were collected and washed with ethanol and deionized water in turn for several times, and then dried in air at 40 ^oC for 12 h.[1, 2]

The pure phase Sr_2YbF_7:Tm^{3+} NCs were prepared *via* the above procedure when x = 0.4, changing Tm^{3+} usage from 0.4% to 0.8%.

S1.3 *In vitro* UC fluorescent bioimaging

The UCNCs@PEG with concentration of 250 μg/mL were incubated with HeLa cells at 37 ^{o}C for 0.5 h under 5% CO_2. After washed with PBS for three times, the cells were visualized under a confocal laser scanning microscope (ZEISS710) by a laser excitation source of 980 nm.[3, 4]

S1.4 Characterization

The crystal structures of as-prepared samples were characterized by a powder X-ray diffraction (XRD) apparatus (D/Max 2500). The morphology, and element constitution of the samples were characterized by transmission electron microscopy (TEM) and high resolution transmission electron microscopy (HRTEM, JEOL 2100) equipped with an Oxford instrument energy dispersive X-ray spectroscopy (EDS) system at the accelerating voltage of 200 kV. Upconversion emission spectra were recorded by a fluorescence spectrophotometer (R500) under the excitation of a 980 nm laser. [4, 5] The surface structure of PEG-modified NCs was tested by Fourier transform infrared spectra (Vertex80+Hyperion2000/Vertex80+ Hyperion2000).

S2. The characterization of as-prepared (1-x)SrF_2•$x$$YbF_3$

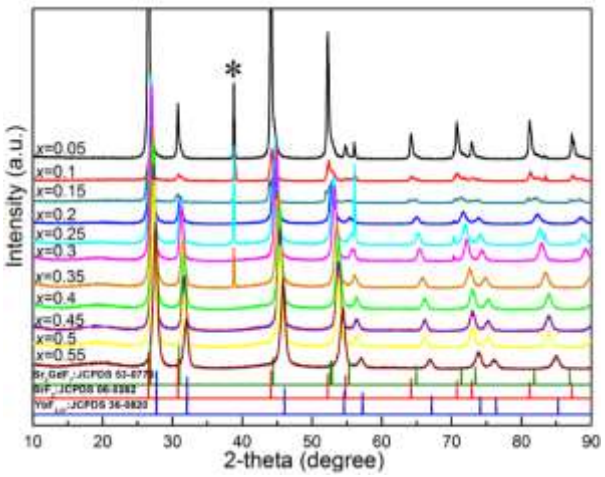

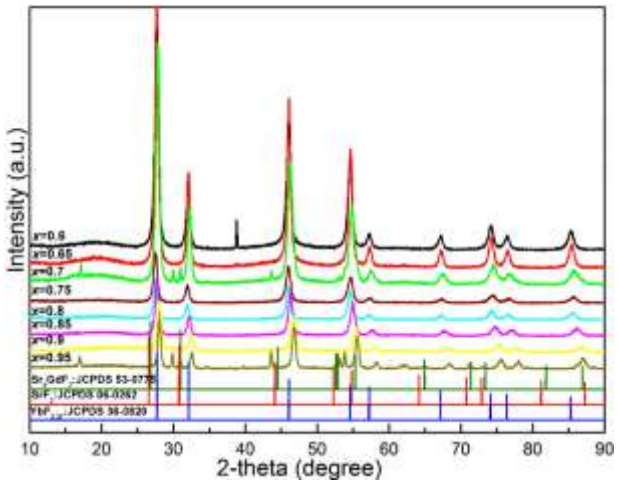

Fig. S1. XRD patterns of (1-*x*)SrF_2•*x*YbF_3 synthesized: 0.05 ≤ *x* ≤ 0.95.

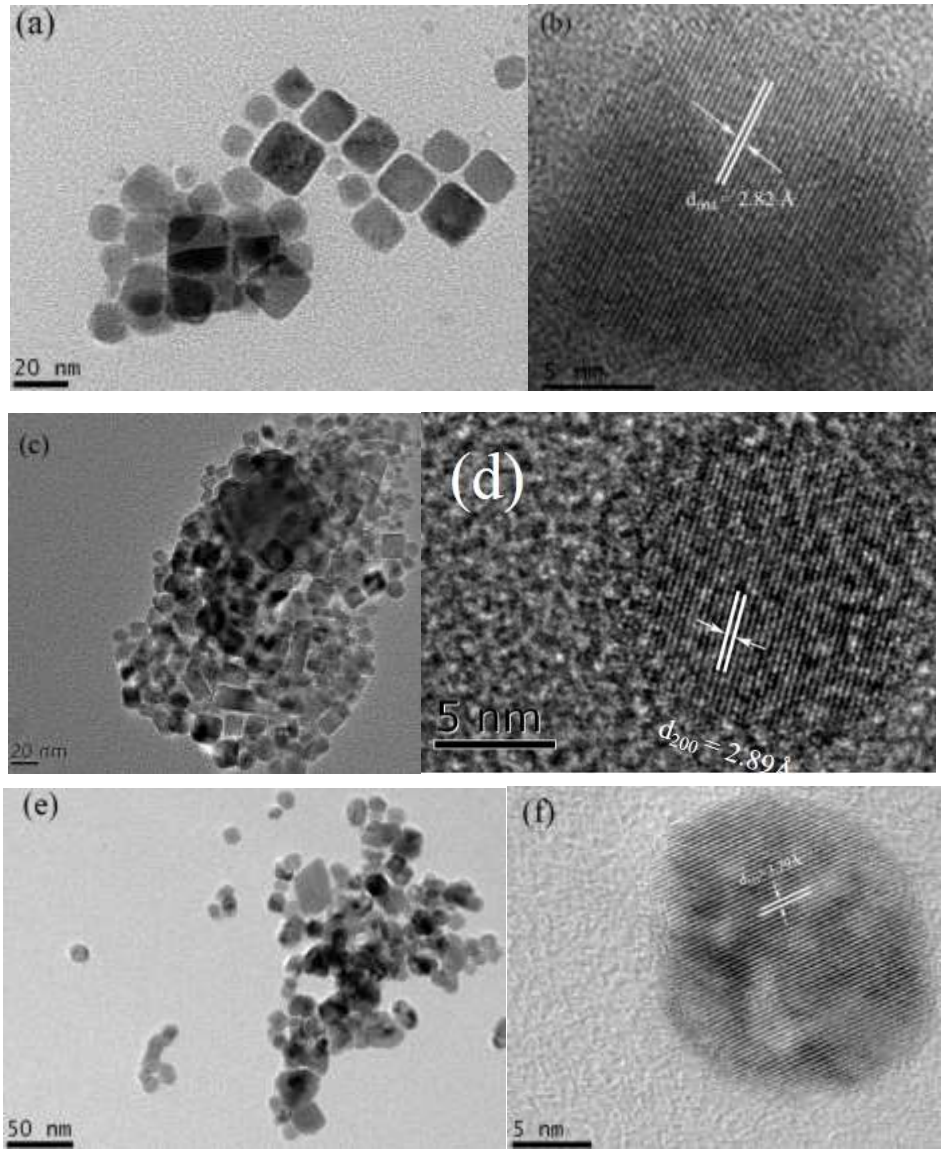

Fig. S2. TEM and HRTEM images of (1-*x*)SrF_2•*x*YbF_3 synthesized: (a and b) *x* = 0.4, (c and d) *x* = 0.1, (e and f) *x* = 0.9.

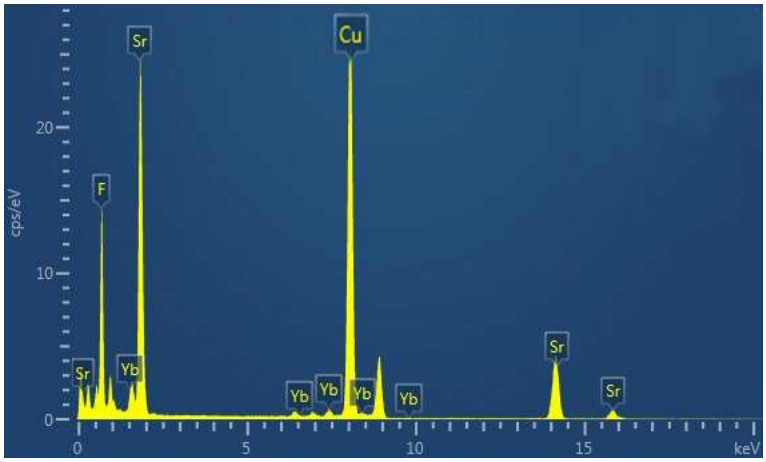

Fig. S3. EDS spectra of (1-*x*)SrF_2•*x*YbF_3 (*x* = 0.4)

Fig. S3 shows the EDS spectra of (1-*x*)SrF_2•*x*YbF_3 (*x* = 0.4). Sr, Yb and F elements could be found in the nanocrystals without other elements.

By tuning the molar ratio of Yb^{3+} to Sr^{2+} ions, a series of (1-*x*)SrF_2•*x*YbF_3 ($0.05 \leq x \leq 0.95$, *x* represented Yb^{3+} content.) NCs were prepared, and phase structure of SrF_2-YbF_3 system was investigated. **Fig. 1** presents the typical XRD patterns of samples synthesized under the similar conditions except Yb^{3+} and Sr^{2+} ions content, which demonstrates the dependence of phase structure of products on the molar ratio of Yb^{3+} to Sr^{2+} ions. When $0.05 \leq x \leq 0.35$, the diffraction peaks were almost consistent, and the products were the mixture of cubic $YbF_{2.37}$ phase (JCPDS 36-0820), cubic SrF_2 phase (JCPDS 06-0262) and some unknown phases (marked as *).

With the increase of *x*, all the diffraction peaks shifted to larger Bragg angle. When $x \geq 0.4$, the diffraction peak * disappeared. The data of the literature [6] was used as a reference. When $0.4 \leq x \leq 0.5$ (Fig.1), these peaks were found to be similar to diffraction data of JCPDS 53-0775 just with a slight shifted to larger Bragg angle [6]. Owing to the smaller radius of Yb^{3+} (0.0858 nm) than Gd^{3+} (0.0938nm), it could be considered the products were pure Sr_2YbF_7 phase [6]. Therefore, when $0.4 \leq x \leq 0.5$, namely, the molar ratio of Sr^{2+} to Yb^{3+} was between 3 : 2 and 1: 1, the products were pure Sr_2YbF_7 phase.

When $x = 0.55$, the products were cubic $YbF_{2.37}$ phase (JCPDS 36-0820). As shown in **Fig. 1**, when $x \geq 0.55$, the products were not pure Sr_2YbF_7 phase. When $0.6 \leq x \leq$

0.7, some random peaks appeared, the products were mixture phase at these conditions. When x = 0.75, the diffraction peaks also were consistent with diffraction data of cubic $YbF_{2.37}$. With the increase of x, namely, $0.8 \leq x \leq 0.95$, all the diffraction peaks continued to gradually move to the right. When x = 0.95, the products were the mixture of hexagonal $NaYbF_4$ phase (JCPDS 27-1427) and other unknown phases.

Then, TEM, HRTEM and EDS(**Fig. S2** and **3**) were used to further investigate the effects of Yb^{3+} content. The TEM and HRTEM images of $(1-x)SrF_2 \bullet xYbF_3$ (x = 0.4) revealed the NCs in relatively uniform shape with the size of about 15 nm and the measured inter-planar distances was about 2.82 Å, corresponding to the (004) lattice plane of tetragonal Sr_2YbF_7, which was consistent with previous XRD results. In addition, the TEM and HRTEM images of $(1-x)SrF_2 \bullet xYbF_3$ (x = 0.1 and 0.9) NCs indicate also the products were mixture.

Fig. S2c-d and **S2e-f** were the TEM and HRTEM images of $(1-x)SrF_2 \bullet xYbF_3$ (x = 0.1 and 0.9) NCs. As shown in Fig.3 (a, c), the crystalline size distribution of the product was bimodal, i.e, and the ultrasmall NCs coexisted with larger NCs. According to the XRD results shown in Fig.1, the ultrasmall NCs primarily belonged to SrF_2 NCs, the measured interplanar distances were about 2.89 Å, corresponding to the (200) lattice plane of cubic SrF_2. While the large NCs were almost $YbF_{2.37}$ NCs and its size was about 30 nm, the measured interplanar distances were about 3.28 Å, corresponding to the (111) lattice plane of cubic $YbF_{2.37}$, which were consistent with XRD results. The EDS spectra of $Sr_{1-x}Yb_xF_{2+x}$ (x = 0.4) showed Sr, Yb and F elements could be found in the nanocrystals without other elements (**Fig. S3)**.

As demonstrated above, the Yb^{3+} content affects the synthesis of pure phase Sr_2YbF_7, and just apropos molar ratio of Sr^{2+} to Yb^{3+} (3:2 to 1:1), namely x = 0.4-0.5, facilitated the formation of pure Sr_2YbF_7 phase with uniform size distribution. Thus, the following experiments used the $(1-x)SrF_2 \bullet xYbF_3$ materials as x = 0.4.

S3 The characterization of Sr_2YbF_7: Tm^{3+} NCs

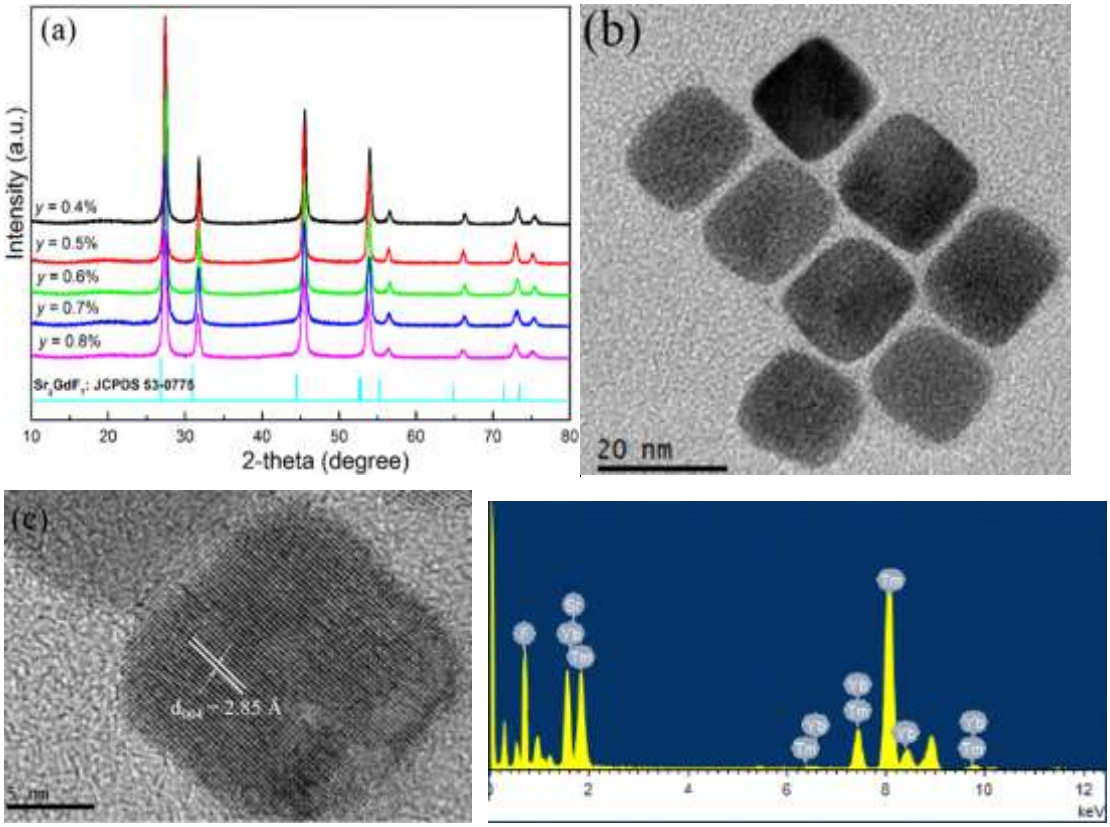

Fig. S4. XRD patterns, TEM, HRTEM and EDS images of Sr_2YbF_7: Tm^{3+} NCs.

To generate upconversion luminescence, Tm^{3+} was chosen as luminescence ions. So, Sr_2YbF_7 was prepared with the different concentration of Tm^{3+} ions doped. **Fig. S4a** shows the typical XRD patterns of Sr_2YbF_7: Tm^{3+} (*y* mol%). The diffraction peaks of XRD patterns are consistent, and similar to diffraction data of JCPDS 53-0775 [5]. The result indicates that the products are pure phase, and the introduction of minor rare-earth ions has little influence on the preparation of pure phase Sr_2YbF_7 NCs. The TEM images (**Fig. S4b**) shows the size of Tm^{3+}-doped Sr_2YbF_7 NCs with uniform shape are about 15 nm. As shown in Fig.3c, the measured interplanar distances is 2.85 Å, corresponding to the (004) lattice plane of Tm^{3+}-doped Sr_2YbF_7, which is close to the interplanar distances of Sr_2YbF_7 (2.82 Å) as mentioned above. The results of the XRD, TEM, HRTME and EDS **(Fig. S4**) indicate that Tm^{3+} ions successfully enter the Sr_2YbF_7 lattice.

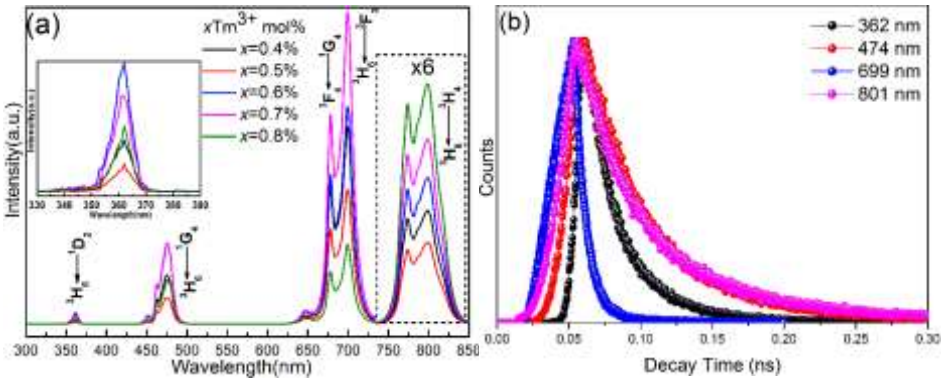

Fig. S5. (a) UC emission spectra of Sr_2YbF_7: Tm^{3+} (y mol%) NCs; (b) The luminescence decays of the UCNCs@PEG.

S4 Fluorescence images of HeLa cells co-labelled with the UCNCs@PEG

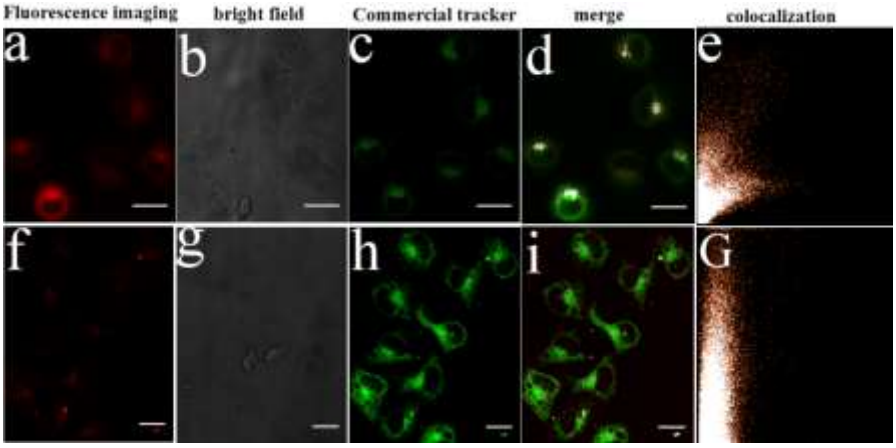

Fig. S6 Fluorescence images of HeLa cells co-labelled with the UCNCs@PEG, Mito tracker (a-e) and Er tracker (f-G). Scale bar = 20 μm.

S5 The thermogravimetric analysis of the UCNCs@PEG

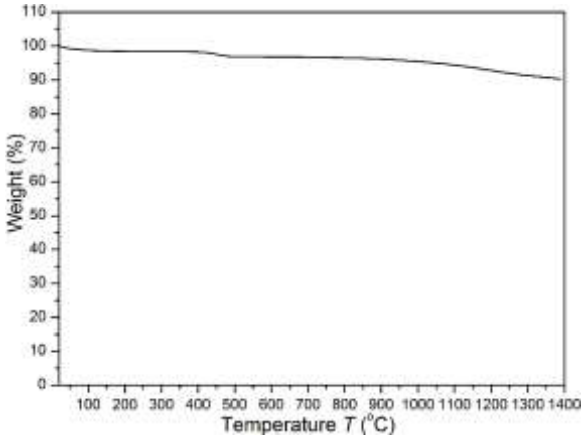

Fig. S7 TGA curve of the UCNCs@PEG

TGA curve of the UCNCs@PEG (Fig. S7) showed the weight loss of the sample was about 9% at 1260 ^{o}C. After this point, no events can be seen until 1400 °C, which indicates that the UCNCs@PEG were exhibiting thermal stability.

References

1 L. J. Xiang, G. Z. Ren, Y. F. Mao, J. He and R. Su, *Optical Materials*, 2015, 49, 6.

2 Y. F. Mao, M. Ma, L. J. Gong, C. F. Xu, G. Z. Ren and Q. B. Yang, *Journal of Alloys and Compounds*, 2014, 609, 262.

3 J. Zhou, Z. Liu and F.Y. Li, *Chem. Soc. Rev*., 2012, 41, 1323.

4 J.C. Colmenares, M.A. Aramendia, A. Marinas, J.M. Marinas and F.J. Urbano, *Appl. Catal. A Gen*., 2006, 306, 120.

5 Y.N. Tang, W.H. Di, X.S. Zhai, R.Y. Yang and W.P. Qin, *ACS Catal*., 2013, 3, 405.

6 X. M. Li, J. K. Cao, Y. L. Wei, Z. R. Yang, and H. Guo, *J. Am. Ceram. Soc*., 2015, 98, 3824.